ADVANCED MATERIALS
www.advmat.de

Pendant Group Functionalization of Cyclic Olefin for High Temperature and High-Density Energy Storage

Stuti Shukla, Chao Wu, Ankit Mishra, Junkun Pan, Aaron P. Charnay, Ashish Khomane, Ajinkya Deshmukh, Jierui Zhou, Madhubanti Mukherjee, Rishi Gurnani, Pragati Rout, Riccardo Casalini, Rampi Ramprasad, Michael D. Fayer, Priya Vashishta, Yang Cao, and Gregory Sotzing**

High-temperature flexible polymer dielectrics are critical for high density energy storage and conversion. The need to simultaneously possess a high bandgap, dielectric constant and glass transition temperature forms a substantial design challenge for novel dielectric polymers. Here, by varying halogen substituents of an aromatic pendant hanging off a bicyclic mainchain polymer, a class of high-temperature olefins with adjustable thermal stability are obtained, all with uncompromised large bandgaps. Halogens substitution of the pendant groups at para or ortho position of polyoxanorborneneimides (PONB) imparts it with tunable high glass transition from 220 to 245 °C, while with high breakdown strength of 625–800 MV/m. A high energy density of 7.1 J/cc at 200 °C is achieved with *p*-POClNB, representing the highest energy density reported among homo-polymers. Molecular dynamic simulations and ultrafast infrared spectroscopy are used to probe the free volume element distribution and chain relaxations pertinent to dielectric thermal properties. An increase in free volume element is observed with the change in the pendant group from fluorine to bromine at the para position; however, smaller free volume element is observed for the same pendant when at the ortho position due to steric hindrance. With the dielectric constant and bandgap remaining stable, properly designing the pendant groups of PONB boosts its thermal stability for high density electrification.

1. Introduction

Climate change and fossil fuel depletion make the grid-level adoption of renewable energies more important now than ever before, and energy storage and conversion technologies play an important role in these initiatives.[1,2] The ultrahigh power density of capacitors makes it irreplaceable for instant energy storage, and there has been increasing demand for capacitors that can be used in elevated temperatures, such as automobiles, aviation, oil, and gas, and space exploration, etc., for harsh conditions and/or higher power and energy densities.[3–7] As such, the dielectric thin films sandwiched between electrodes that hold opposite charges to store electrostatic energies are required to withstand temperatures above 150 °C and even 250–300 °C, e.g., the operating temperature of hybrid electric vehicles (≈140–150 °C), aerospace (≈150–350 °C), oil and gas exploration (≈170–250 °C), etc.[8,9] While dielectric materials of capacitors can be inorganics, polymers are preferred due to their

S. Shukla, P. Rout, G. Sotzing
Department of Chemistry
University of Connecticut
Storrs, CT 06269, USA
E-mail: g.sotzing@uconn.edu
C. Wu[+], J. Zhou, Y. Cao
Electrical and Computer Engineering
University of Connecticut
Storrs, CT 06269, USA
E-mail: yang.cao@uconn.edu
The ORCID identification number(s) for the author(s) of this article can be found under https://doi.org/10.1002/adma.202402133
[+]Present address: Department of Electrical Engineering, Tsinghua University, Beijing 100084, China

DOI: 10.1002/adma.202402133

A. Mishra, P. Vashishta
Collaboratory for Advanced Computing and Simulations
Department of Chemical Engineering and Materials Science
Department of Physics and Astronomy
and Department of Computer Science
University of Southern California
Los Angeles, CA 90089, USA
J. Pan, A. P. Charnay, M. D. Fayer
Department of Chemistry
Stanford University
Stanford, CA 94305, USA
A. Khomane, A. Deshmukh
Institute of Materials Science
University of Connecticut
Storrs, CT 06269, USA

flexibility, light weightiness, cost-effective processability, and, most of all, their voltage scalability and graceful failure mode, which prevents any abrupt failure.[10,11] The maximum energy density of the capacitor can be determined using the following equation[12]

$$U = \frac{1}{2}\varepsilon_0 \varepsilon E^2 \quad (1)$$

where U is the energy density, $\mathcal{E}_0$ is vacuum permittivity, $\mathcal{E}$ is the dielectric constant, and E is the breakdown strength.

Currently, the most common commercially used dielectric polymer is the biaxially oriented polypropylene (BOPP).[13] BOPP has a high breakdown strength of 700 MV m^{-1}, a bandgap of ≈7 eV, and a dielectric constant of 2.2. However, the maximum operating temperature of BOPP is ≈85 °C, above which the soaring conduction loss and hence largely reduced dielectric strength will necessitate significant derating and/or cumbersome active cooling, resulting in poor overall energy density and efficiency.[14] Many high-temperature polymer systems have been investigated as dielectric materials to obviate cooling systems. However, common high-temperature dielectric polymers have an aromatic ring present in their backbone,[15,16] which causes a low bandgap and leads to loss at high electric field. A dielectric material with higher bandgap would require more energy for an electron to "travel" from the valence to the conduction band, contributing to higher breakdown strength. According to Equation (1), the higher breakdown strength is beneficial to higher energy density. Aliphatic polymers such as polyethylene and polypropylene have a large bandgap, but they have low glass transition temperatures. In some previously published works, an inverse correlation between bandgap and glass transition temperature has been shown.[17] To break this design constraint, a new polymer system was introduced, and they have both high glass transition temperature and bandgap, called poly oxanorbornenes (PONBs).[18] They have a high bandgap due to the absence of π–π stacking in the polymer backbone and the introduction of a saturated rigid bicyclic ring to the polymer backbone. This backbone with restricted mobility in the polymer backbone helped to give a higher bandgap (> 4.5 eV). A higher glass transition temperature was obtained by further limiting the segmental mobility by introducing a bulky benzene ring side chain with the imide. This class of dielectric polymers has glass transition temperature (≈180–250 °C) and bandgaps above 4.5 eV. They were easy to synthesize and to cast into flexible thin polymer films. This system serves a good candidate for high-temperature dielectric materials for capacitive energy storage.[19,20]

The breakdown of a dielectric material is a complex phenomenon. However, large bandgaps and high glass transition temperatures are important in determining intrinsic breakdown strength. There are of course other extrinsic parameters, such as chemical impurity, defects, film quality, morphology, etc.[21,22] Other ways to improve the breakdown strength of a material include the introduction of inorganic materials with large bandgap to make a composite or as a coating. These methods also have drawbacks in terms of flexibility, processability, cost, etc.[23] Composites are not preferred sometimes due to their uneven distributions of inorganic material and brittleness after scaling up which can lead to lower electrical performance or early breakdown under long-term harsh conditions operation.[24] Copolymers are also used as dielectric materials, while the design and optimization of copolymers are still based on homo-polymers.[25] These give all organic homo-polymers an advantage over composites, plasma coatings, and copolymers. The energy density of a capacitor is directly proportional to the dielectric constant and square of breakdown strength, which means that understanding breakdown strength will help to improve the energy density of the capacitor.

There have been previous studies where polar groups were introduced to the polymer structure to affect the energy density and efficiency of the polymer.[26,27] However, there has not been any systematic studies on the effect of halogen addition on the structural, thermal, and dielectric properties of the polymers that work under high temperature as well as high electric field. In this work, the systematic addition of halogens (F, Cl, Br) as the pendant group at the para and ortho position to the benzene ring attached to the imide ring of polyoxanorbornene and its correlation to the material and electrical properties are studied. Ortho-POBrNB was not part of this study. Bromine being larger in size and a good leaving group causes challenges in monomer synthesis at the ortho position. Due to the synthesis and processing difficulties, it is not considered in this work. The key reason and importance of studying dielectric properties of halogenated polynorbornene are that we hope to observe the changes in thermal properties along with the dielectric constant by changing the electronic part of the dielectric constant with systematic addition of halogens of different sizes and electronegativity as a pendant group to benzene.[28] This study is expected to shed a light on the interplays between changes in the size of halogens, polarizability with free volume element (FVM), rotation with halogen addition, and their effects on the dielectric properties of the polymer. The significance of the position of the pendant group to the benzene ring and its effect on the dielectric properties are also interesting targets of this study. Overall, such improved understandings of the breakdown strength of high-temperature dielectric polymers could lead to proper designs of novel high-temperature dielectric polymers.

All of the polymers and monomers, as shown in the reaction and structure schemes in **Figure 1**a,b, were synthesized in our laboratory using a similar method as mentioned in some previously published works.[29–31] Nuclear magnetic resonance spectroscopy (NMR) was used for structural confirmation as well as the purity check of the monomer and polymer. Detailed materials characterizations of all monomers as well as polymers are shown in Figures S1–S21 of the Supporting Information. The free-standing polymer film, as shown in Figure 1c, was processed using a solution casting method with the help of a doctor blade film coater. These polymers show a large bandgap, which was

M. Mukherjee, R. Gurnani, R. Ramprasad
School of Materials Science and Engineering
Georgia Institute of Technology
Atlanta, GA 30332, USA
R. Casalini
Chemistry Division
US Naval Research Laboratory
Washington, DC 20375, USA

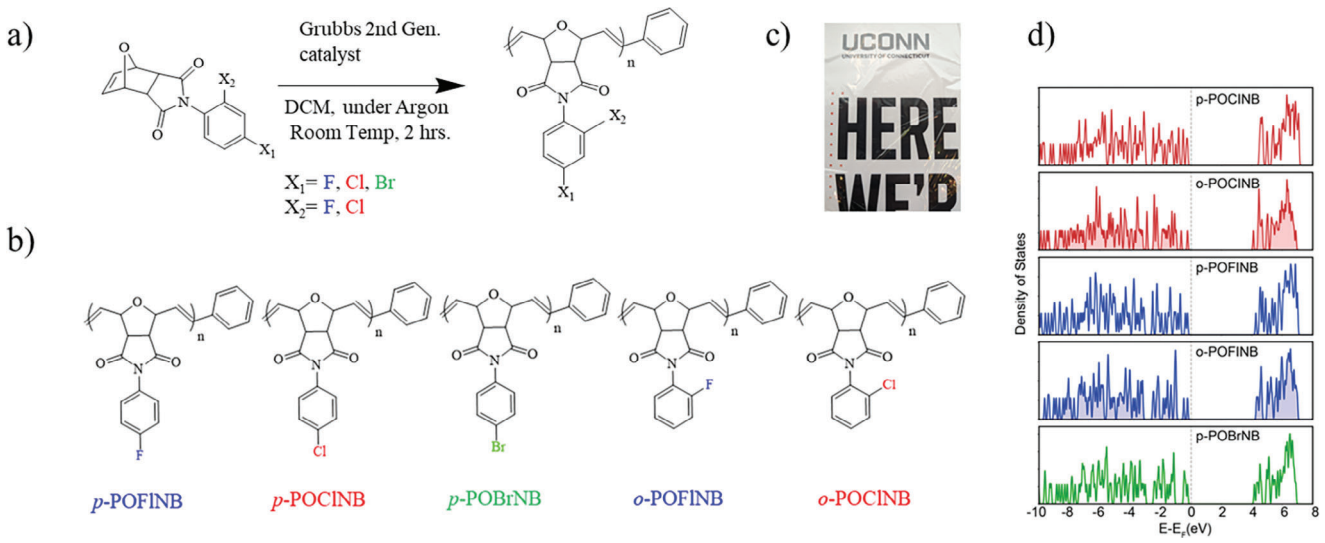

Figure 1. Materials. a) Polymer synthesis scheme of Polyoxanorbornenes. b) halogenated polyoxanorbornenes structures (POXNB) (X = F, Cl, Br). c) Free-standing thin film of p-POClNB. d) The electronic density of states of POXNBs, computed based on density functional theory.

confirmed by the computed electronic density of states, as shown in Figure 1d. In particular, p-POCINB shows the largest bandgap of 4.7 eV among all POXNBs.

The 5% degradation temperature (T_d) of all polymers is above 350 °C, which shows good thermal stability. The T_g of POXNB increases as the size of the halogen atom and free volume element increase in the case of both paras as well as ortho-substituted halogens, as shown in **Figure 2a**. It shall be noted that these measurements of FVE radii of these halogen substituted PONBs were conducted at room temperature in glassy state well below their glass transition temperatures. However, if we compare the T_g of ortho- and para-substituted POClNB or POFlNB, we can see that ortho substituents have higher T_g than that of para substituents, as we can see in Table S1 (Supporting Information),

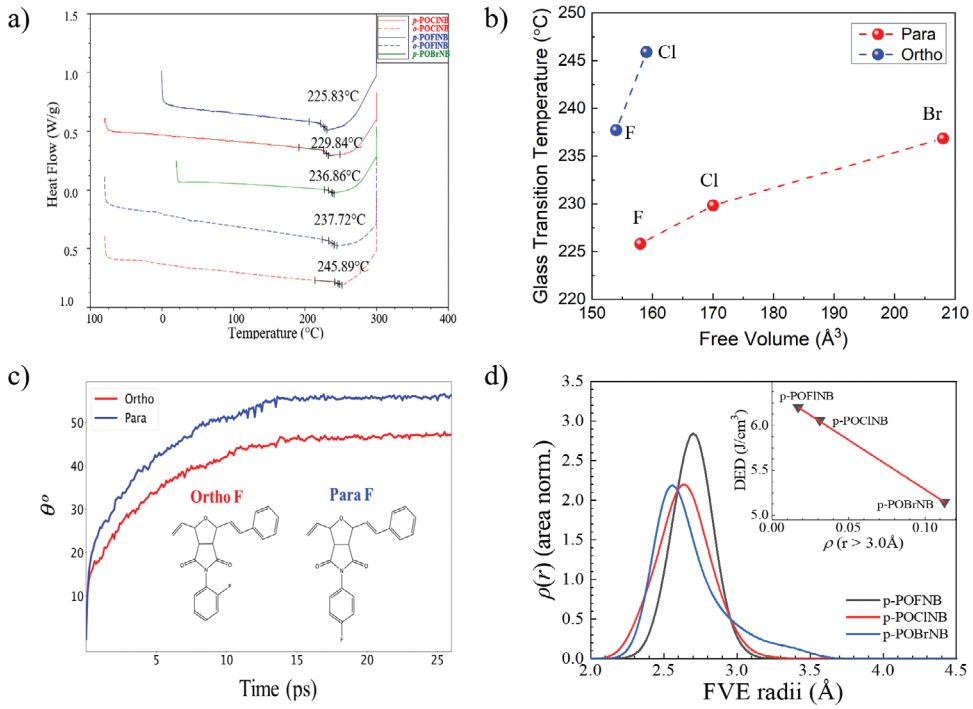

Figure 2. Thermal properties. a) Glass transition temperature of halogenated Polyoxanorbornenes (p, o-POXNB). b) Free volume element versus T_g of halogenated polynorbornenes. c) Rotation analysis of ortho and para – POFlNB. d) Radius probability distributions (RPDs) of p-POXNBs free volume elements. The inset depicts the correlation of discharge energy density at a field strength of ≈700 MV m^{-1} to the probability of having large FVE radius. *x*-axis is the integral of the radius probability distribution function from 3 Å to infinity. The red line is drawn for visual guidance only.

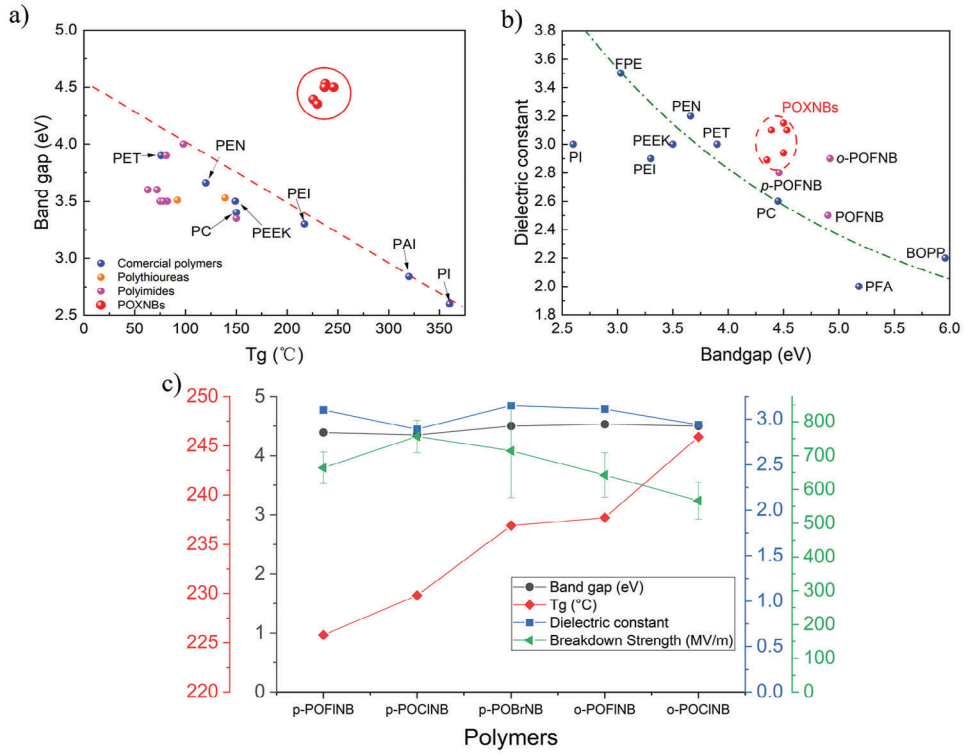

Figure 3. Key parameters and their relationship. a) T_g versus bandgap of halogenated polynorbornenes in comparison to commercial high-temperature polymers. b) Bandgap versus Dielectric Constant of POXNBs compared to other Dielectric Polymers. c) Bandgap, glass transition temperature, dielectric constant, and breakdown strength for polymers investigated.

which is caused by the restricted rotation of ortho substituents in the presence of imide. It can be seen from Figure 2b that free volume element increases as we change pendant halogens from F to Cl to Br group with an increase in the T_g at both ortho as well as para positions. Furthermore, it can be seen that free volume element at the ortho position is lower than that of the para position due to steric hindrance of the side groups that couples its motion to that of the backbone restricting the rotation of the benzene ring. The rotation analysis for these halogenated polymers was performed by observing the rotation of the benzene rings to which pendant halogens attach at ortho and para positions. A comparison of various ortho as well as para groups for F Cl and Br in Figure 2c and Figures S22–S23 (Supporting Information) demonstrates that para reaches the θ position faster and the saturated θ is bigger compared to ortho due to restriction in rotation for ortho caused by the imide group. From a combination of the linear absorption spectrum and the frequency-dependent radii extracted from ultrafast anisotropy measurements, the area-normalized radius probability distribution (RPD) of free volume element (FVE) radii for the three para-substituted POXNBs is extracted (Figure 2d). Figure S24 (Supporting Information) highlights the differences in the long tails of the FVE RPDs. The peaks of the distribution shift to the smaller radius side when the size of the para-substituent increases; on the contrary, the probability of having the larger FVE radius has the opposite trend (Br > Cl > Fl).[32,33]

The energy density of dielectric polymers is quadratically dependent on the breakdown strength and proportional to the dielectric constant. Although the breakdown process is complicated, previous studies indicated that the breakdown strength is positively dependent on the bandgap. **Figure** 3a shows the relationship of bandgaps and glass transition temperatures for the polymers investigated here and reported. Due to the saturated backbone structure, POXNBs have concurrently high bandgaps and high glass transition temperatures relative to traditional aromatic high temperature dielectric polymers. The dielectric constant of dielectric polymers is also inversely related to the bandgap due to the exclusive relationship between the bandgap and electronic dielectric constant, as shown in Figure 3b. Halogenated polymers here have a relatively high dielectric constant in comparison to commercial polymers or POFNBs. Due most likely to the fact the smaller single halogen groups relative to the CF_3 group in POFNBs can reorient more easily, the dielectric constant of POXNBs is higher. Overall, there is no major significant change in the dielectric constant of the halogenated polymers at 100 Hz at room temperature (Figures S25 and S26, Supporting Information). The bandgap, glass transition temperature, dielectric constant, and breakdown strength for polymers as a function of different halogens and positions are shown in Figure 3c and Figures S25–S28 (Supporting Information). Dielectric constant and bandgap varied slightly when the halogens and their positions change. With the increasing of the atomic number for both orthos and paras, the glass transition temperature increased. The higher glass transition temperature is beneficial to higher breakdown strength at 200 °C as the bandgap is close for the five polymers. However, the breakdown strength

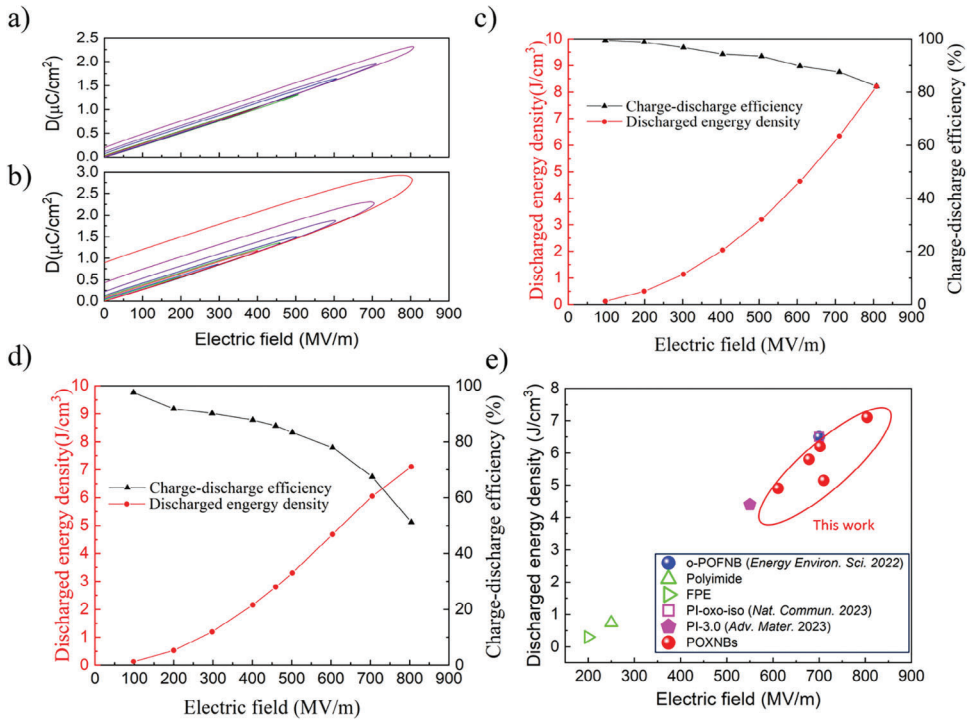

Figure 4. High field energy storage performance of p-POClNB. a,b) at 150 and 200 °C DE loop. c,d) Discharge energy density and charge–discharge efficiency of p-POClNB at 150 and 200 °C. e) 200 °C comparison of POXNBs and other published all-organic pure homopolymers.

exhibits complicated relationship with the halogens and their positions. In our previous study that investigated PEIs modified with different endcaps, we proposed a correlation between the probability of having large FVE to the dielectric breakdown strength of the polymers.[32] The theoretical rationale for this model is based on the Artbauer model of dielectric breakdown in polymers,[33] which suggests that the largest FVEs in a given polymer are the ones in which dielectric breakdown takes place. In this model, electrons in an FVE are accelerated by the applied field (F) and have a certain probability of tunneling into a neighboring FVE (P_μ) according to the kinetic energy of the electron when it encounters the potential barrier of the FVE wall (E_μ). The larger the size of FVE, the longer the mean free path of an electron in that FVE (x). Hence the higher the kinetic energy at the wall and the higher the probability of tunneling (Equation (2)). It would therefore be predicted that polymers with a greater fraction of large FVEs (Figure S24, Supporting Information) will tend to have lower dielectric breakdown strength and lower energy density as the dielectric constants are similar, which suggests p-POFlNB should have the highest breakdown strength and highest discharge energy density which goes as the square of dielectric breakdown strength. The prediction holds very well for the discharge energy density (see inset Figure 2d) which provides experimental support for the Artbauer model but does not predict the ordering of the dielectric breakdown strengths themselves. Rational design of new polymer with high breakdown strength should simultaneously consider the impacts of bandgap, glass transition temperature, free volume elements, and mechanical factors. The stronger steric hindrance of the side groups for ortho-PONBs may suppress the degree of freedom of the chain movement, contributing toward lower breakdown strength due to mechanical factors. As the bandgap is similar, probably the competitive influence of free volume element and glass transition temperature gives rise to the highest breakdown strength for p-POClNB

$$P_\mu = e^{\frac{-\left(E_\mu - eFx\right)}{kT}} \tag{2}$$

The discharged energy density was measured using the D–E hysteresis loop analysis, as shown in **Figure 4** and Figure S27 (Supporting Information). The area between charging and discharging cycles in the D–E loop analysis shows the total energy loss during the process, and a slim loop means higher efficiency. Total energy loss increases with the increase of free volume element for halogens of F and Cl relative to Br at the para position, while there are no major changes in the case of F and Cl for the close free volume element Figure 2b. It can also be observed from Figure S27 (Supporting Information) that in the case of ortho, total energy loss decreases from F to Cl (SI) due to the increase of the free volume element. This pattern can also be supported by our previous work, in that polymers with pendant $-CF_3$ group at the para position have high loss and low charge–discharge efficiency even at 150 °C because of higher free volume element than that of pendant Br group.[19] With well-balanced free volume element, glass transition temperature, and large bandgap, p-POClNB has the highest energy density of 7.1 J cc^{-1} at 200 °C, the highest among reported all-organic homopolymers.

2. Conclusion

To summarize, the effect of the systematic addition of halogens as a pendant group at the ortho and para position of high-temperature poly oxanorbornenes on structural, thermal, and electrical properties was successfully studied. High-purity monomers, as well as polymers, were synthesized and processed using the solution casting method to get free-standing polymer films. It is well known that going down on the periodic table group VIIA, the size of the atom increases and the electronegativity decreases. The addition of the halogens as a pendant group at para and ortho position affects multiple properties of high temperature dielectric polymers. The free volume element increases with the increase of the size of halogens. Halogens at ortho positions contribute to smaller free volume element and higher glass transition temperature due to the restriction in rotation of the pendant halogen group. Electrical parameters of these polymers showed no significant change in the case of dielectric constant and bandgap. With well-balanced structural, thermal, and electrical parameters, one of the polymers investigated, p-POClNB, exhibits the highest energy density of 7.1 J cc^{-1} at 200 °C. These discoveries provide a framework to design polymers with high energy density and thermal resistance by modularly designing their backbone and pendant separately. It is also discussed that the overall contribution of the molecular structure, free volume element, thermal and electrical parameters should be considered simultaneously when exploring a new high temperature dielectric polymer.

3. Experimental Section

Materials: Starting materials Exo-3,6-epoxy-1,2,3,6-tetrahydro phthalic anhydride (Oxanorbornene anhydride), anhydrous toluene, dichloromethane (DCM), tetrahydrofuran (THF), methanol, ethanol, acetic anhydride Anhydrous sodium acetate, 4-flouroaniline. 4-chloroaniline. 4-bromoaniline, 2-flouroaniline, and 2-chloroaniline were purchased from Fisher Scientific. Grubbs generation 2 catalyst was used for ring-opening metathesis polymerization (ROMP) and was purchased from Sigma-Aldrich.

Characterization: ^{1}H and ^{19}F NMR (Nuclear magnetic resonance) analysis was studied for structural characterization of synthesized monomers as well as polymers with the help of Bruker AVANCE 500 MHz spectrometer using TMS as an internal standard (Figures S29–S43, Supporting Information). Glass transition Temperatures (T_g) of polymers were measured using differential scanning calorimetry (DSC) using TA instruments DSC Q29 with heating and cooling rates of 10 °C min^{-1}. Degradation of polymer was analyzed with the help of thermogravimetric analysis (TGA) using TA instruments TGA Q-500 with a heating rate of 20 °C min^{-1} up to 650–700 °C. PerkinElmer's Lambda 1050 UV/VIS/NIR spectrometer was used to conduct ultraviolet–visible spectroscopy to calculate the bandgap of the polymers. Restricted orientation anisotropy method (ROAM) was employed for characterizing the free volume element distributions, as described below.

Rotational Barrier and Free Volume Calculations: The rotational barrier calculation was done by rotating the pendant group with respect to the polymer backbone to create the initial geometries. The geometries thus obtained had polymer backbone orientations almost similar across all the structures. The rotated pendant groups were then structurally optimized at very low temperatures using a polarizable reactive molecular dynamics-based force field. This force field has been previously fitted to[34–39] Polynorbornene and various other polymers to obtain correct ground state configurations. The molecular dynamics calculation using this force-field was done with conjugate gradient-based optimization, which relaxes the structure to its lowest energies. Thus, various structures obtained were relaxed, and the rotational profile was obtained for halogenated polymers.

The free volume with respect to the pendant group was done using Voronoi-based free volume analysis. Here, a molecular dynamics box of the most relaxed polymer orientation, as obtained from the above step, was amorphized to the desired density of 1.2 gm cc^{-1}. The simulation here was done at room temperature to allow the polymer chains enough kinetic freedom. Then a voronoi volume was drawn across each pendant group, and its volume fraction was measured with respect to the entire molecular dynamics box. The Voronoi package **voro++** for this calculation and **Ovito** visualization software for structure generation and analysis were utilized.[40–42]

Restricted Orientation Anisotropy Method (ROAM): Free volume element (FVE) distributions of the para-substituted POXNBs were characterized using a recently developed method based on ultrafast infrared spectroscopy, called restricted orientation anisotropy method (ROAM). A detailed description of the method has been published previously.[43,44] Here, a brief overview of the method will only be given. The main observable for ROAM is the anisotropy decay of the vibrational probes embedded in the polymer matrix, which was measured using polarization selective pump–probe spectroscopy (PSPP). Anisotropy is a measurement of time-dependent orientational relaxation of the probe molecules. In a nonviscous liquid, the anisotropy would decay to zero at a long time as the excited population fully randomizes its orientation, but in the polymer matrix, the anisotropy decays to a constant offset, since the probes molecules are confined by the walls of the FVEs, and only sample a limited range of angles. Furthermore, in polymer the anisotropy decay is frequency-dependent, which means that there are subensembles of probe molecules experiencing different degrees of confinement. If the FVE as a cylindrical cone was modeled, these angles can readily be extracted by fitting the anisotropies to the well-established wobbling-in-a-cone (WIAC) model.[45–47] The extracted angles are called "half cone angles" and are directly related to the size of the FVE. However, to make the result more easily interpretable, the size of the PhSeCN molecule was modeled and the half cone angles into FVE radii were converted. The length of the PhSeCN molecule is determined using DFT calculation, and radii of the moiety colliding with the walls are the Van der Waals radii by Bondi.[48] It is worth noting that the comparison made with the ROAM result is true regardless of what length model is used, since it is essentially based on the cone angles. The change of different probe size modeling would only shift the exact numbers of the radii. Once the radii are determined at each frequency, this result can be combined with the linear absorption spectrum (the probability distribution of the frequency) to extract FVE radii distribution in the sample using the maximum entropy method.

Bandgap Calculations: Density of states and bandgap calculations were performed using first-principles density functional theory as implemented in the Vienna ab initio simulation package (VASP).[49,50] The halogen polymers were modeled as oligomers with two repeat units to manage the computational cost. The structures of these polymers were optimized using Perdew–Burke–Ernzerhof XC functional with projector augmented wave (PAW) potentials to represent the electron–ion interactions. The complete optimization of the structures was achieved by employing a conjugate gradient scheme until the components of forces on individual atoms were less than 0.02 eV $Å^{-1}$. A plane-wave energy cutoff of 500 eV was used for all the structures. After geometry optimization, the structures were further converged by using strict energy convergence criteria of 10^{-6} eV to ensure accuracy. To obtain an accurate density of states, the Heyd–Scuseria–Ernzerhof hybrid density functional (HSE06) was used.[51]

Electrical Characterizations: The dielectric constant and dissipation factor were measured using Solartron 1296 dielectric interfaces. DE loops were measured using a modified Sawyer-Tower polarization tester. The 100 Hz unipolar positive half sinusoidal waveform was amplified to apply high-voltage on the film to get the charging–discharging loops.

Supporting Information

Supporting Information is available from the Wiley Online Library or from the author.

Acknowledgements

S.S. and C.W. contributed equally to this work. This work was supported through a Multidisciplinary University Research Initiative (MURI) Grant (No. N00014-17-1-2656) and a capacitor program Grant (No. N0014-19-1-2340), both from ONR.

Conflict of Interest

The authors declare no conflict of interest.

Data Availability Statement

The data that support the findings of this study are available from the corresponding authors upon reasonable request.

Keywords

breakdown, electronic bandgap, free volume, glass transition, polymer dielectrics

Received: February 8, 2024
Revised: April 28, 2024
Published online:

[1] T. Kousksou, P. Bruel, A. Jamil, T. E. L. Rhafiki, Y. Zeraouli, *Sol. Energy Mater. Sol. Cells* **2014**, *120*, 59.
[2] P. F. Ribeiro, B. K. Johnson, M. L. Crow, A. Arsoy, Y. Liu, *Proc. IEEE* **2001**, *89*, 1744.
[3] J. Ho, T. R. Jow, S. Boggs, *IEEE Electr. Insul. Mag.* **2010**, *26*, 20.
[4] B. K. Kim, S. Sy, A. Yu, J. Zhang, *Handbook of Clean Energy Systems*, John Wiley & Sons Ltd, Chichester, UK **2015**, p. 1–25. https://doi.org/10.1002/9781118991978.hces112
[5] W. J. Sarjeant, I. W. Clelland, *Proc. IEEE* **2001**, *89*, 846.
[6] H. D. Abruña, Y. Kiya, J. C. Henderson, *Phys. Today* **2008**, *61*, 43.
[7] B. Fan, F. Liu, G. Yang, H. Li, G. Zhang, S. Jiang, Q. Wang, *IET Nanodielectr.* **2018**, *1*, 32.
[8] R. W. Johnson, J. L. Evans, P. Jacobsen, J. R. Thompson, M. Christopher, *IEEE Trans. Electron. Packag. Manuf.* **2004**, *27*, 164.
[9] J. A. Weimer, *Proceedings of the IEEE/AIAA Digital Avionics Systems Conference*, IEEE, Fort Worth, TX **1993**, pp. 445–450. https://doi.org/10.1109/DASC.1993.283509.
[10] Q. Li, L. Chen, M. R. Gadinski, S. Zhang, G. Zhang, H. Li, A. Haque, L. Q. Chen, T. Jackson, Q. Wang, *Nature* **2015**, *523*, 576.
[11] V. Sharma, C. Wang, R. G. Lorenzini, R. Ma, Q. Zhu, D. W. Sinkovits, G. Pilania, A. R. Oganov, S. Kumar, G. A. Sotzing, S. A. Boggs, R. Ramprasad, *Nat. Commun.* **2014**, *5*, 4845.
[12] T. Zhang, X. Chen, Y. Thakur, B. Lu, Q. Zhang, J. Runt, Q. M. Zhang, *Sci. Adv.* **2020**, *6*, eaax6622.
[13] J. L. Nash, *Polym. Eng. Sci.* **1988**, *28*, 862.
[14] A. A. Deshmukh, C. Wu, O. Yassin, L. Chen, S. Shukla, J. Zhou, A. R. Khomane, R. Gurnani, T. Lei, X. Liang, R. Ramprasad, Y. Cao, G. Sotzing, *ACS Appl. Mater. Interfaces* **2023**, *15*, 46840.
[15] J. Ho, R. Jow, Army Res Laboratories, DTIC Doc, ARL-TR-4880, https://apps.dtic.mil/sti/tr/pdf/ADA502532.pdf (accessed: July 2009).
[16] G. M. Treich, M. Tefferi, S. Nasreen, A. Mannodi-Kanakkithodi, Z. Li, R. Ramprasad, G. A. Sotzing, Y. Cao, *IEEE Trans. Dielectr. Electr. Insul.* **2017**, *24*, 732.
[17] R. Ma, A. F. Baldwin, C. Wang, I. Offenbach, M. Cakmak, R. Ramprasad, G. A. Sotzing, *ACS Appl. Mater. Interfaces* **2014**, *6*, 10445.
[18] C. Wu, A. A. Deshmukh, Z. Li, L. Chen, A. Alamri, Y. Wang, R. Ramprasad, G. A. Sotzing, Y. Cao, *Adv. Mater.* **2020**, *32*, 200499.
[19] A. A. Deshmukh, C. Wu, O. Yassin, A. Mishra, L. Chen, A. Alamri, Z. Li, J. Zhou, Z. Mutlu, M. Sotzing, P. Rajak, S. Shukla, J. Vellek, M. A. Baferani, M. Cakmak, P. Vashishta, R. Ramprasad, Y. Cao, G. Sotzing, *Energy Environ. Sci.* **2022**, *15*, 1307.
[20] C. Wu, A. A. Deshmukh, O. Yassin, J. Zhou, A. Alamri, J. Vellek, S. Shukla, M. Sotzing, R. Casalini, G. A. Sotzing, Y. Cao, *Proc. Natl. Acad. Sci. USA* **2021**, *118*, 2115367118.
[21] A. Huzayyin, S. Boggs, R. Ramprasad, *IEEE Trans. Dielectr. Electr. Insul.* **2010**, *17*, 926.
[22] Z. Li, C. Wu, L. Chen, Y. Wang, Z. Mutulu, H. Uehara, J. Zhou, M. Cakmak, R. Ramprasad, Y. Cao, *Adv. Mater.* **2024**, *36*, 2310497.
[23] C. A. Grabowski, S. P. Fillery, N. M. Westing, C. Chi, J. S. Meth, M. F. Durstock, R. A. Vaia, *ACS Appl. Mater. Interfaces* **2013**, *5*, 5486.
[24] R. Wang, Y. Zhu, J. Fu, M. Yang, Z. Ran, J. Li, M. Li, J. Hu, J. He, Q. Li, *Nat. Commun.* **2023**, *14*, 2406.
[25] J. Chen, Y. Zhou, X. Huang, C. Yu, D. Han, A. Wang, Y. Zhu, K. Shi, Q. Kang, P. Li, P. Jiang, X. Qian, H. Bao, S. Li, G. Wu, X. Zhu, Q. Wang, *Nature* **2023**, *615*, 62.
[26] M. R. Gadinski, Ph.D. Thesis, The Pennsylvania State University **2015**.
[27] J. Mao, S. Wang, Y. Cheng, B. Xiao, L. Zhang, D. Ai, Y. Chen, W. Sun, J. Luo, *Chem. Eng. J.* **2022**, *444*, 136331.
[28] G. Cavallo, P. Metrangolo, R. Milani, T. Pilati, A. Priimagi, G. Resnati, G. Terraneo, *Chem. Rev.* **2016**, *116*, 2478.
[29] K. Mizuta, S. Fukutomi, K. Yamabuki, K. Onimura, T. Oishi, *Polym. J.* **2010**, *42*, 534.
[30] A. A. Santiago, J. Vargas, S. Fomine, R. Gaviño, M. A. Tlenkopatchev, *J. Polym. Sci. A: Polym. Chem.* **2010**, *48*, 2925.
[31] S. Çetinkaya, R. Bayram, *Heteroat. Chem.* **2010**, *21*, 36.
[32] S. M. Fica-Contreras, Z. Li, A. Alamri, A. P. Charnay, J. Pan, C. Wu, J. R. Lockwood, O. Yassin, S. Shukla, G. Sotzing, Y. Cao, M. D. Fayer, *Mater. Today* **2023**, *67*, 57.
[33] J. Artbauer, *J. Phys. D: Appl. Phys.* **1996**, *29*, 446.
[34] A. Mishra, L. Chen, Z. Li, K.-I. Nomura, A. Krishnamoorthy, S. Fukushima, S. C. Tiwari, R. K. Kalia, A. Nakano, R. Ramprasad, G. Sotzing, Y. Cao, F. Shimojo, P. Vashishta, *Comput. Mater. Sci.* **2023**, *228*, 112340.
[35] A. L. Nazarova, L. Yang, K. Liu, A. Mishra, R. K. Kalia, K. Nomura, A. Nakano, P. Vashishta, P. Rajak, *J. Chem. Inf. Model.* **2021**, *61*, 2175.
[36] A. Mishra, S. Hong, P. Rajak, C. Sheng, K. Nomura, R. K. Kalia, A. Nakano, P. Vashishta, *NPJ Comput. Mater.* **2018**, *4*, 42.
[37] A. Krishnamoorthy, A. Mishra, N. Grabar, N. Baradwaj, R. K. Kalia, A. Nakano, P. Vashishta, *Comput. Phys. Commun.* **2020**, *254*, 107337.
[38] A. Alamri, C. Wu, A. Mishra, L. Chen, Z. Li, A. Deshmukh, J. Zhou, O. Yassin, R. Ramprasad, P. Vashishta, Y. Cao, G. Sotzing, *Chem. Mater.* **2022**, *34*, 6553.
[39] A. Krishnamoorthy, A. Mishra, D. Kamal, S. Hong, K. Nomura, S. Tiwari, A. Nakano, R. Kalia, R. Ramprasad, P. Vashishta, *SoftwareX* **2021**, *13*, 100663.
[40] C. H. Rycroft, Ph.D. Thesis, Massachusetts Institute of Technology **2007**.
[41] C. H. Rycroft, *Chaos* **2009**, *19*, 041111.
[42] A. Stukowski, *Model Simul. Mater. Sci. Eng.* **2009**, *18*, 015012.
[43] S. M. Fica-Contreras, D. J. Hoffman, J. Pan, C. Liang, M. D. Fayer, *J. Am. Chem. Soc.* **2021**, *143*, 3583.

[44] D. J. Hoffman, S. M. Fica-Contreras, M. D. Fayer, *Proc. Natl. Acad. Sci. USA* **2020**, *117*, 13949.
[45] G. Lipari, A. Szabo, *Biophys. J.* **1980**, *30*, 489.
[46] H. S. Tan, I. R. Piletic, M. D. Fayer, *J. Chem. Phys.* **2005**, *122*, 174501.
[47] G. Lipari, A. Szabo, *J. Am. Chem. Soc.* **1982**, *104*, 4546.
[48] A. Bondi, *J. Phys. Chem.* **1964**, *68*, 441.
[49] G. Kresse, J. Furthmüller, *Comput. Mater. Sci.* **1996**, *6*, 15.
[50] M. Fuchs, M. Scheffler, *Comput. Phys. Commun.* **1999**, *119*, 67.
[51] J. Heyd, G. E. Scuseria, M. Ernzerhof, *J. Chem. Phys.* **2003**, *118*, 8207.